Available online at www.sciencedirect.com
ScienceDirect
Trans. Nonferrous Met. Soc. China 34(2024) 3777−3788
Transactions of Nonferrous Metals Society of China
www.tnmsc.cn

Effects of anode slime removing by Fe^{2+} dissolution method on electrochemical properties of Pb−0.6%Ag anode and zinc electrowinning

Wen-jun WANG[1,2,3], Lan-bo LI[1], Xu LIU[4], Tie-chui YUAN[1], He-xin GAO[1]

1. State Key Laboratory of Powder Metallurgy, Central South University, Changsha 410083, China;
2. Zhejiang Libo Industrial Co., Ltd., Shaoxing 312000, China;
3. College of Mechanical and Energy Engineering, Shaoyang University, Shaoyang 422000, China;
4. Zhuzhou Smelter Group Co., Ltd., Zhuzhou 412000, China

Received 12 September 2023; accepted 28 April 2024

Abstract: Fe^{2+} dissolution method and manual method were used to remove the anode slime and their effects on properties of cast Pb−0.6wt.%Ag anode and zinc electrowinning were compared. The results reveal that the Fe^{2+} dissolution method can avoid mechanical damage to the oxide film layer on the anode surface, which cannot be achieved by traditional manual method. This can lower the anode corrosion rate by 57.14%, thus reducing Pb contamination in electrolyte and zinc products. Meanwhile, compared with manual method, Fe^{2+} dissolution method can significantly improve the electrocatalytic activity of the anode and lower the initial power consumption of zinc electrowinning to 2720 kW·h/t after removing anode slime.

Key words: Pb−Ag anode; zinc electrowinning; anode slime removing; electrochemical properties

1 Introduction

Zinc electrowinning, as one of the key procedures of hydrometallurgy, determines many critical indicators such as zinc product quality, power consumption, and anode consumption [1−4]. During zinc electrowinning, the oxygen evolution reaction occurs on the surface of lead-based silver-containing (0.2−1.0 wt.%) anode, and the metal on the anode surface is slowly transformed into oxide [5−7]. The existence of the oxide layer on the anode surface helps reduce the oxygen evolution potential and maintain the zinc electrowinning power consumption at a low level, nevertheless, the lead-containing compounds on the anode surface will partially dissolve into the electrolyte, thus deteriorating the quality of zinc products [8,9]. In order to control the Pb contamination of cathode zinc products and keep the anode from quick corrosion, 3−5 g/L of Mn^{2+} is constantly added into the zinc electrolyte [10,11].

During zinc electrowinning, Mn^{2+} in the electrolyte is oxidized into MnO_2, which forms anode slime with other metal oxides on the anode surface [10,12]. The excessive accumulation of anode slime on the anode surface not only reduces the conductivity of the anode, but also intensifies the concentration polarization of the solution, thus increasing the zinc electrowinning power consumption [13,14]. In addition, excessive accumulation of anode slime is prone to cause short-circuits between the anode and cathode, which will accelerate the anode corrosion rate and significantly decrease the service life of the anode, thus elevating the lead content in zinc products [15]. In order to solve the above problems in industrial zinc electrowinning, it is necessary to regularly

Corresponding author: Tie-chui YUAN, Tel/Fax: +86-731-88830142, E-mail: tiechuiyuan@csu.edu.cn
DOI: 10.1016/S1003-6326(24)66640-9

remove the anode slime on the anode surface (Ranging from 15 to 45 d). Although the addition of Mn^{2+} to the electrolyte can lower the anode corrosion rate, it still consumes about 2 kg of anode metal when 1 t of zinc is obtained [16]. This indicates that a large amount of anode slime will inevitably form and cause Pb pollution to the environment during the transferring and treating processes [17,18].

For zinc electrowinning enterprises, thousands or even tens of thousands of anodes are required to serve in the electrolysis cell, and most enterprises use manual removing method to remove anode slime on plate piece by piece, which poses the following prominent problems for enterprises: (1) a large amount of human resources will be wasted; (2) the harsh working environment of workers poses a highly potential risk to their health; (3) it is easy to cause residual stress in the anode, which tends to cause short-circuits between the anode and cathode; (4) it is prone to cause damage to the anode surface oxide film and even the metal matrix, resulting in the short and the uneven service life of each anode [19].

In recent years, to solve the abovementioned problems, many researchers have conducted investigations on new anodes, new zinc electrowinning methods, and anode pretreatment. In terms of new anodes, intermetallic compound anodes [20,21], metal based coated anodes [22,23], powder anodes [24−26], 3D printed anodes [7], porous anodes [27,28] and polyaniline anode [29] have been proved to be capable of solving the problem of lead pollution and reducing the anodic oxygen evolution overpotential, but their poor mechanical properties and/or complex fabrication process limit their wide application. In terms of new zinc electrowinning methods, diaphragm electrolysis technology [6,30] and NH_4Cl solution electrolysis technology [31] have been proved to be capable of reducing the anodic oxygen evolution overpotential and inhibiting the anodic corrosion rate, but it is difficult to be widely applied due to the complex process and large equipment investment. In the aspect of anode pretreatment, anode pre-coating [9,18] has been proved to help reduce the initial corrosion rate of new anodes, but a series of problems caused by anode slime removing process during long-term service of the anode still remain unsolved.

In this work, Fe^{2+} dissolution method and manual method were used to remove the anode slime, and the impacts of both methods on the anode properties and zinc electrowinning were investigated by anode electrochemical test, scanning electron microscopy, phase analysis of the oxide layer and zinc electrowinning test.

2 Experimental

2.1 Materials and reagents

High-purity water with specific resistance of 0.23 MΩ·cm was used to prepare aqueous solutions. The cast Pb−0.6wt.%Ag alloy anode, the aluminum plate cathode and osseocolla were provided by the Zhuzhou Smelter Group Co., Ltd. The graphite was purchased from the Xinxiang Ruilong New Material Technology Co., Ltd., sulfuric acid (H_2SO_4), zinc sulfate ($ZnSO_4·7H_2O$), ferrous sulphate ($FeSO_4·7H_2O$), and manganese sulfate ($MnSO_4·H_2O$) were of analytical grade and purchased from the Sinopharm Chemical Reagent Co., Ltd.

2.2 Apparatus and procedures

2.2.1 Anode slime forming and removing

Figure 1 exhibits the schematic diagram of the anode slime forming test. The anode slime forming and removing involve the following four main steps: (1) the manufacturing of anodes and cathodes, (2) surface pretreatment, (3) constant current test, and (4) anode slime removing.

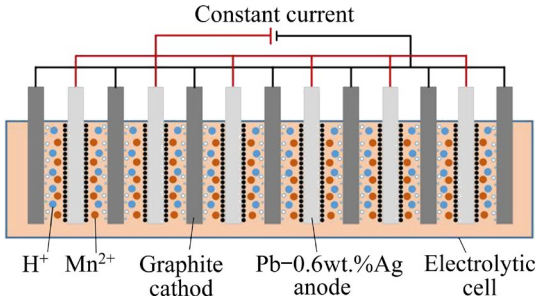

Fig. 1 Schematic diagram of anode slime formation test

Firstly, the cast Pb−0.6wt.%Ag alloy anodes were machined into T-shape with an effective size of 105 mm × 78 mm × 6 mm, and the high purity graphite cathodes were cut into the same size.

Secondly, the surfaces of the anodes were brushed with 600-grit SiC paper to remove superficial impurities like oil and dirt. After brushing, the plates were degreased ultrasonically in deionized water for 5 min and immediately wiped. In the third step, as shown in Fig. 1, the cathodes and anodes were added to the 18 L cell containing 4 g/L Mn^{2+} and 160 g/L H_2SO_4 solution with a circulation speed of 160 mL/min, while the homonymous electrode distance was set at 70 mm for maintaining the solution temperature at (40±0.5) °C, and the solution with $MnSO_4$ and water was regularly added to maintain the concentration of Mn^{2+} at 4 g/L. A current density of 500 A/m^2 was maintained for 21 d to form anode slime on the anode surface. In the fourth step, anodes were removed from the cell and divided into two types. One type is to manually scrape the anode surface with an iron blade to remove the anode slime; the other type is to immerse the anode in a stirring solution containing 20 g/L Fe^{2+} and 70 g/L H_2SO_4 for 3 h and then remove it. Afterwards, it was flushed repeatedly with high-purity water to remove residual solution from the anode surface.

The principle of Fe^{2+} dissolution is exhibited in Reaction (1), that is, MnO_2 in the anode slime is dissolved into Mn^{2+} in the aqueous solution, so that the anode slime on the anode plate falls off, while the inner layer of Pb-containing oxide film on the anode surface remains on the anode surface due to its strong adhesion to the anode metal matrix.

$$MnO_2+2FeSO_4+2H_2SO_4=MnSO_4+Fe_2(SO_4)_3+2H_2O \quad (1)$$

2.2.2 Performance test

As shown in Fig. 2, zinc electrowinning comparison tests were carried out on the manually removed anode (MRA) and the Fe^{2+} dissolution removed anode (DRA) under the same conditions. All cathodes were composed of aluminum, with an effective size of 105 mm × 78 mm × 3 mm. The electrolyte containing 4 g/L Mn^{2+}, 55 g/L Zn^{2+}, 160 g/L H_2SO_4, and 15 mg/L osseocolla was used in the comparison tests, and the experimental parameters for zinc electrowinning are as follows: current density 500 A/m^2, power-on time 24 h, electrolyte temperature (40±0.5) °C, and homonymous electrode distance 70 mm. Power consumption (W) and current efficiency (η) were calculated by Eq. (2) and Eq. (3):

$$W=\frac{UIt}{m} \quad (2)$$

$$\eta=\frac{m}{1.22It}\times 100\% \quad (3)$$

where U is the average input voltage (V), I is the setting current (A), t is power-on time (h), m is the mass of zinc production (g), and 1.22 is the electrochemical equivalent of zinc.

2.2.3 Electrochemical test

A sketch of the electrochemical test anode is shown in Fig. 3(a). The production of test anodes mainly includes the following steps: (1) grinding one side of the MRA and DRA using 600-grit SiC paper until the metal substrate is completely exposed, (2) cutting MRA and DRA into squares with a side length of 10 mm, (3) welding a copper

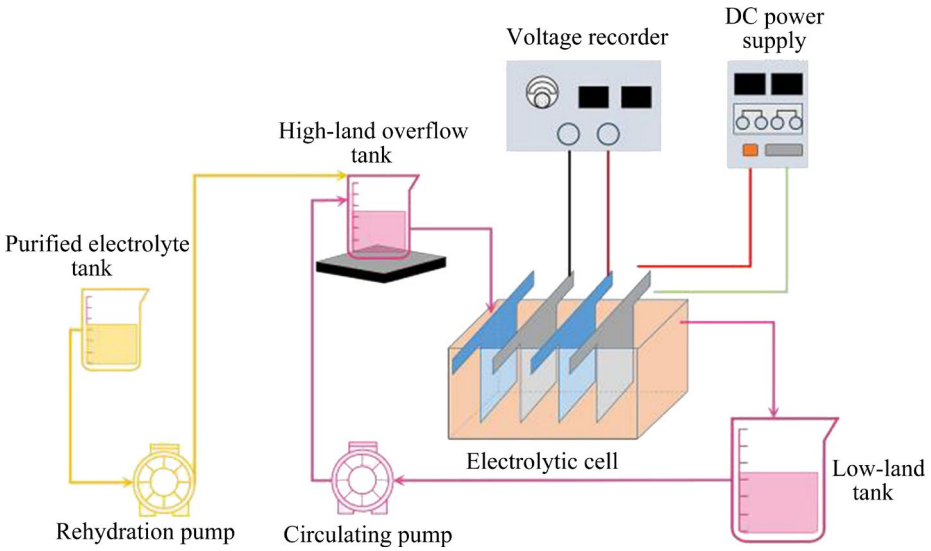

Fig. 2 Schematic diagram of zinc electrowinning device

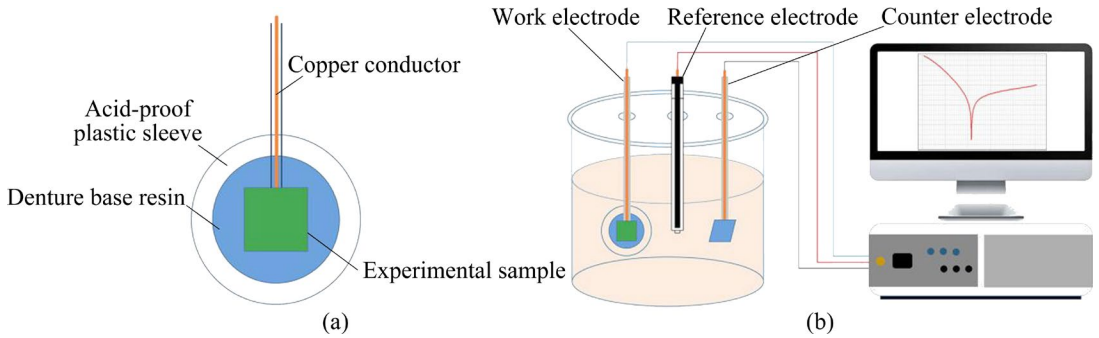

Fig. 3 Schematic diagram of electrochemical test anode (a) and equipment (b)

wire to the metal substrate side with tin, and (4) coating the samples with a denture-based resin with an exposed area of 10 mm × 10 mm.

The anodic polarization, Tafel and cyclic voltammetry measurements were carried out in the solution with 50 g/L Zn^{2+} and 160 g/L H_2SO_4. All electrochemical tests were carried out in a three-electrode cell using an electrochemical workstation (CHI 760E, Huachen, China) at (40±0.5) °C. The counter electrode was a platinum plate with an area of 10 mm × 10 mm, and the reference electrode was a saturated calomel electrode (SCE). The electrochemical experimental device is exhibited in Fig. 3(b). Anodic polarization tests were carried out at a constant scanning rate of 0.5 mV/s from 1.3 to 1.8 V. Tafel curves were obtained at a scanning rate of 3 mV/s. Cyclic voltammetry tests were carried out at a constant scanning rate of 20 mV/s from −1.5 to 2.1 V. All tests were conducted three times to ensure the repeatability.

2.3 Characterization

The Pb content in zinc product and Pb^{2+} concentration in the solution were analyzed by inductively coupled plasma mass spectrometry (ICP-MS). The morphologies of samples were characterized by the SEM (Nova Nano SEM 230). The phases of samples were identified by XRD (Rigaku D/MAX−2250) with Cu K_α radiation.

3 Result and discussion

3.1 Performance comparison

In purpose of comparing the performance of MRA and DRA, these two anodes were tested under the same industrial zinc electrowinning conditions. After each cycle, the zinc products obtained by zinc electrowinning test were cleaned, dried and weighed, the Pb content in zinc and the Pb^{2+} concentration in the electrolyte were measured, and the power consumption and current efficiency were calculated using Eq. (2) and Eq. (3), respectively. The MRA and DRA were dried and weighed before zinc electrowinning tests. After which, MRA and DRA were immersed in a stirring solution containing 20 g/L Fe^{2+} and 70 g/L H_2SO_4 for 3 h, and then washed with deionized water, dried carefully at a constant temperature of 60 °C for 24 h and weighed to obtain the anodic mass loss. The results are exhibited in Table 1 and Table 2.

The Pb^{2+} concentration in the electrolyte is less than 0.01 mg/L before the service of anode (Table 1). However, after one cycle of service, the concentrations of Pb^{2+} in the corresponding electrolytes of DRA and MRA are significantly increased, indicating that the anode metal is corroded and dissolved in the electrolyte during the oxygen evolution process. In addition, as exhibited in Table 1, the content of Pb in zinc and the Pb^{2+} concentration in electrolyte corresponding to each cycle of DRA are significantly lower than those of MRA.

For MRA, in the first cycle, the Pb^{2+} concentration in the electrolyte is 0.49 mg/L and the lead content in zinc with MRA is 0.0076 wt.%. This means the lead content in zinc products is significantly higher than the national standard for $0^{\#}$ grade zinc with a 0.003 wt.% Pb [27], which is mainly attributed to the crush of a large portion of oxide layer on the anode surface during manual removing process, leaving the anode metal matrix exposed in the electrolyte, thus resulting in the dissolution of a large amount of lead in the solution and reduction at the cathode [4,30]. But for DRA, in the first cycle, attributing to the intact anodic

surface oxide layer, the Pb^{2+} concentration in the electrolyte is 0.26 mg/L, which corresponds to nearly half of MRA, while the lead content in zinc products is only 0.0018% and meets the national standard for 0# grade zinc [27].

Table 1 Comparison of MRA and DRA in terms of Pb content in zinc product, Pb^{2+} concentrations in electrolyte and anodic mass loss

Anode	Cycle No.	Pb^{2+} concentration in electrolyte/ ($mg·L^{-1}$)	Pb content in zinc product/ wt.%	Anodic mass loss/g
MRA	0	<0.01	−	−
MRA	1	0.49	0.0076	−
MRA	2	0.23	0.0016	−
MRA	3	0.15	0.0006	4.27
DRA	0	<0.01	−	−
DRA	1	0.26	0.0018	−
DRA	2	0.15	0.0006	−
DRA	3	0.15	0.0005	1.83

Table 2 Comparison of MRA and DRA in terms of current efficiency and power consumption

Anode	Cycle No.	Zinc mass/g	Current efficiency/%	Power consumption/ ($kW·h·t^{-1}$)
MRA	1	409.6	90.02	3142
MRA	2	404.7	88.95	2875
MRA	3	405.1	89.03	2872
DRA	1	409.8	90.07	2720
DRA	2	403.9	88.77	2870
DRA	2	404.5	88.90	2873

As the second and third cycles of zinc electrowinning proceed, the anode slime layer on the anode surface gradually thickens, and the Pb^{2+} concentration in electrolyte and Pb content in the zinc product gradually decrease. In contrast, because of the complete retention of the oxide film on the surface of DRA, the Pb^{2+} concentration in the electrolyte and Pb content in the zinc product in each cycle are significantly lower than those of MRA. It is worth noting that the anodic mass loss of MRA is 2.33 times that of DRA after three cycles of zinc electrowinning, indicating the lower anode corrosion rate of DRA compared with MRA by 57.14%, which is mainly attributed to the crush of MRA film layer. This indicates that the Fe^{2+} dissolution method can effectively inhibit Pb pollution and prolong the service life of anode.

As exhibited in Table 2, the zinc mass and current efficiency of each cycle of MRA and DRA are similar, so is the power consumption of the second and third cycles, while the power consumption of the first cycle of MRA and DRA is significantly varied (The power consumption of MRA in the first cycle is 422 kW·h/t higher than that of DRA). As we all know, zinc electrowinning power consumption is directly related to the anode surface film and the integrity of the film layer [10,16]. Attributing to the mechanical damage of MRA, the surface film is destroyed, while the surface lead oxide film of DRA is well preserved, that is, MRA needs to be re-formed in the process of zinc electrowinning, so the power consumption of MRA in the first cycle is significantly higher than that of DRA, and with the progress of the second and third cycles, the anode surface film gradually becomes stable. Therefore, the second and third cycles of MRA and DRA are similar.

3.2 Electrochemical behavior

3.2.1 Cell voltage

For comparing the electrocatalytic activity of MRA and DRA, the variation of cell voltage in the first cycle of zinc electrowinning is presented in Fig. 4, which illustrates that the cell voltages of MRA and DRA exhibit significantly different variation trends. The initial cell voltage of MRA is 3.346 V, which drops rapidly in the initial stage of zinc electrowinning. Afterwards, the decline rate gradually decreases and is finally stabilized at about 3.0 V. The initial cell voltage of DRA is 2.792 V, which shows a rapid increase in the initial stage of zinc electrowinning. As zinc electrowinning proceeds, the cell voltage of DRA slowly rises and is finally stabilized at about 3.0 V. It is well known that the electrocatalytic activity of the anode oxide layer directly determines the cell voltage and the zinc electrowinning power consumption [16,32]. The above results are consistent with the power consumption results of MRA and DRA in the first cycle in Section 3.1.

As for MRA, attributing to the break of the surface film, the catalytic activity of the anode surface is poor while the initial cell voltage is high.

As the oxygen evolution reaction on the anode surface proceeds, the catalytic active film on the anode surface is gradually formed by oxidizing the surface metal of the anode, and the cell voltage gradually decreases and finally becomes stable. For DRA, the high electrocatalytic activity film layer is intact and the initial cell voltage is low. As the oxygen evolution reaction on the anode surface proceeds, the manganese dioxide on the anode surface gradually grows in the highly electrocatalytic active film and gradually forms a coating, which elevates the cell voltage and finally becomes stable [10,12].

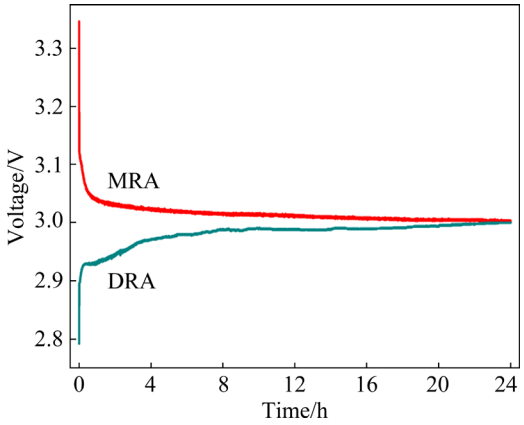

Fig. 4 Cell voltages of MRA and DRA

3.2.2 Anodic polarization curves

To further explore and compare the oxygen evolution catalytic activity of MRA and DRA, anodic polarization curves are plotted and the relevant results are presented in Fig. 5, which indicates that the polarization terminal current density of DRA is significantly higher than that of MRA. This is consistent with the highest current density obtained in CV testing while is opposite to the initial cell voltage in zinc electrowinning testing. Figure 5 also shows that the current density of DRA gradually increases when the potential exceeds 1.5 V, while the current density of MRA gradually rises when the potential exceeds 1.65 V. This elucidates that the oxygen evolution catalytic activity of DRA is superior to that of MRA.

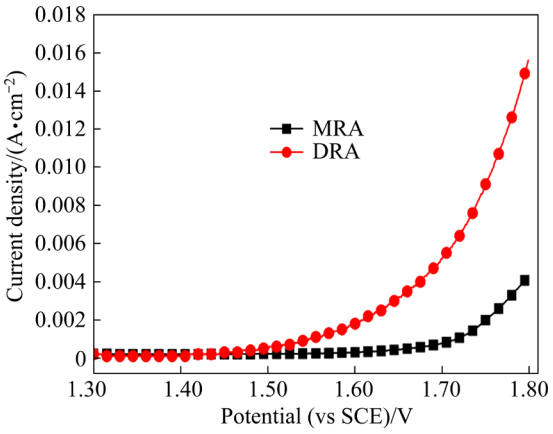

Fig. 5 Anodic polarization curves of MRA and DRA

3.2.3 Tafel curves

To explore the reasons for the variation in corrosion resistance between MRA and DRA, the Tafel curves were plotted and the results are exhibited in Fig. 6. The corrosion potential (φ_{corr}) and the corrosion current density (J_{corr}) are extracted by performing linear fitting of the Tafel curves (Fig. 6) and the relevant results are listed in Table 3. It can be observed that DRA has higher φ_{corr} (1.096 V (vs SCE)) and lower J_{corr} (1.32×10^{-7} A/cm^2). In general, J_{corr} is often used to judge the corrosion resistance of the anode: under the same conditions, a smaller J_{corr} value indicates a better corrosion resistance of the anode [10]. Therefore, the corrosion resistance of DRA is obviously better than that of MRA, which may be because the oxidation layer on the surface of DRA is relatively intact, while that on the surface of MRA is mostly destroyed.

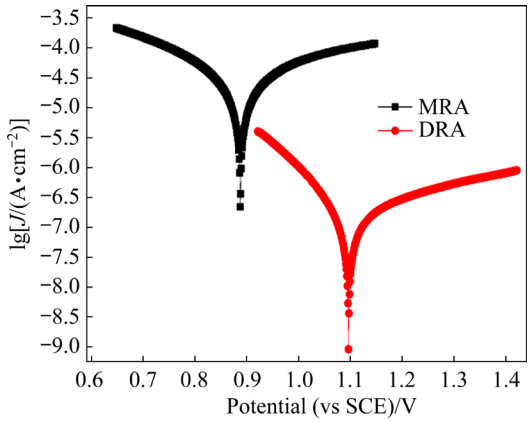

Fig. 6 Tafel curves of MRA and DRA

Table 3 Corrosion potentials and corrosion current densities of different anodes

Anode	φ_{corr}(vs SCE)/V	J_{corr}/(A·cm^{-2})
MRA	0.862	2.96×10^{-5}
DRA	1.096	1.32×10^{-7}

3.2.4 CV curves

To further investigate the electrochemical mechanism of MRA and DRA, the cyclic voltammetry curves were measured and the results

are exhibited in Fig. 7, in which O1, O2, and O3 represent different oxidation reactions, while R1 and R2 represent different reduction reactions. The corresponding principles are as follows: O1 represents the oxidation reaction from Pb to $PbSO_4$; O2 represents the oxidation reaction from $PbSO_4$ to PbO_2 and oxygen evolution reaction; O3 represents the oxidation reaction from Pb to $PbSO_4$ inside the oxide layer of anodes through cracks and pores of the oxide layer; R1 represents the reduction reaction from PbO_2 to $PbSO_4$; R2 represents the reduction reaction from $PbSO_4$ to Pb [8,33].

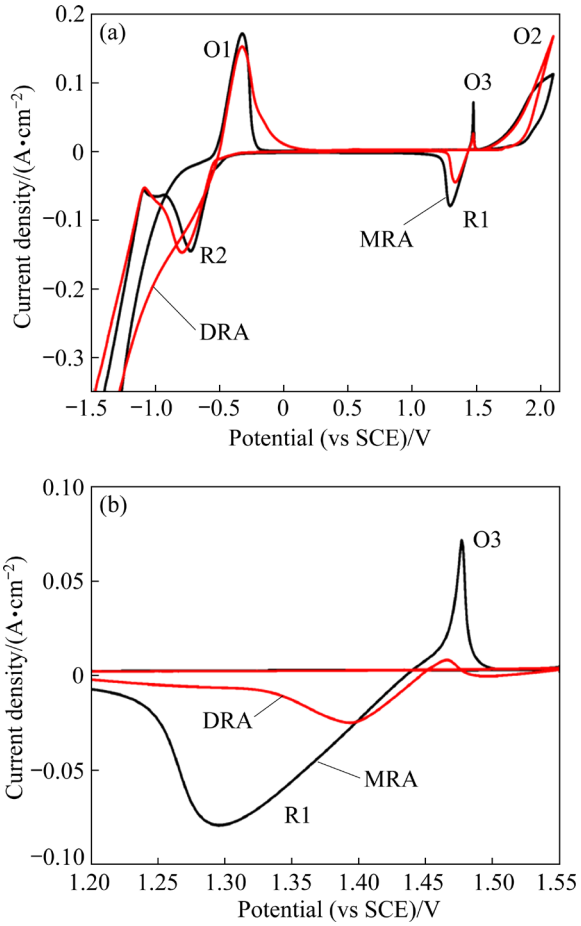

Fig. 7 Cyclic voltammetry curves of MRA and DRA (a), and enlarged view of peak O3 and R1 (b)

Figure 7 indicates that DRA and MRA have significant differences in each absorption peak. The peak intensity of DRA at O1 is significantly weaker than that of MRA, which is mainly because the film layer of DRA is completely preserved, which effectively prevents the corrosion of the anode metal matrix. This is also the main reason why the anodic mass loss of DRA is obviously lower than that of MRA. The peak intensity of DRA at O2 is predominantly higher than that of MRA, which may be attributed to the complete and highly catalytic oxidation film layer on the surface of DRA, thus promoting oxygen evolution reaction [1]. The peak intensity of DRA at O3 is notably weaker than that of MRA, which indicates that the complete oxidation film layer on DRA can effectively protect the anode metal matrix from further corrosion [8].

3.3 Surface morphology and phase composition

3.3.1 Surface morphology

To compare the surface morphologies of MRA and DRA as well as those of MRA and DRA after galvanostatic polarization at 500 A/m^2 for 24 h, SEM and corresponding EDS tests were conducted and the relative results are exhibited in Fig. 8 and Fig. 9, respectively, which indicates that there are significant differences in the surface morphologies between MRA and DRA, and the variation becomes slight after galvanostatic polarization. Figure 8(a) illustrates that some areas on the surface of MRA are smooth with clearly visible residual particles, while some areas are uneven and exhibit disordered clumps. Besides, there are obvious scratches at the junction of the uneven and smooth areas.

Figures 9(a−c) and Fig. 10 illustrate that the MRA surface is mainly composed of PbO and residual granular $PbSO_4$. Figure 8(b) indicates that the surface of DRA is mainly composed of particles with varying sizes. Combining Figs. 9(d, e) with Fig. 10, it can be observed that the particles of varying sizes are mainly $PbSO_4$, α-PbO_2, β-PbO_2 and PbO. Figures 8(c, d) show that there are two types of oxides on the anode surface after galvanostatic polarization: one is loose coral-like oxide, which grows on the outer surface of the anode; the other is smooth and dense large particle that grows on the bottom layer of loose coral-like oxides. Combining Figs. 9(f−i) with Fig. 10, it can be speculated that these two types of oxides with various shapes are MnO_2.

It can be seen from Fig. 8(a) that the surface oxide of MRA is completely destroyed, while Fig. 8(b) shows that the surface oxide of DRA remains relatively intact. For MRA, attributing to the fragment of the surface oxide layer, the anode surface needs to oxidize the metal substrate on the anode surface to form a stable oxide layer when the anode is in service, which will accelerate the anode corrosion process and shorten the service life of the

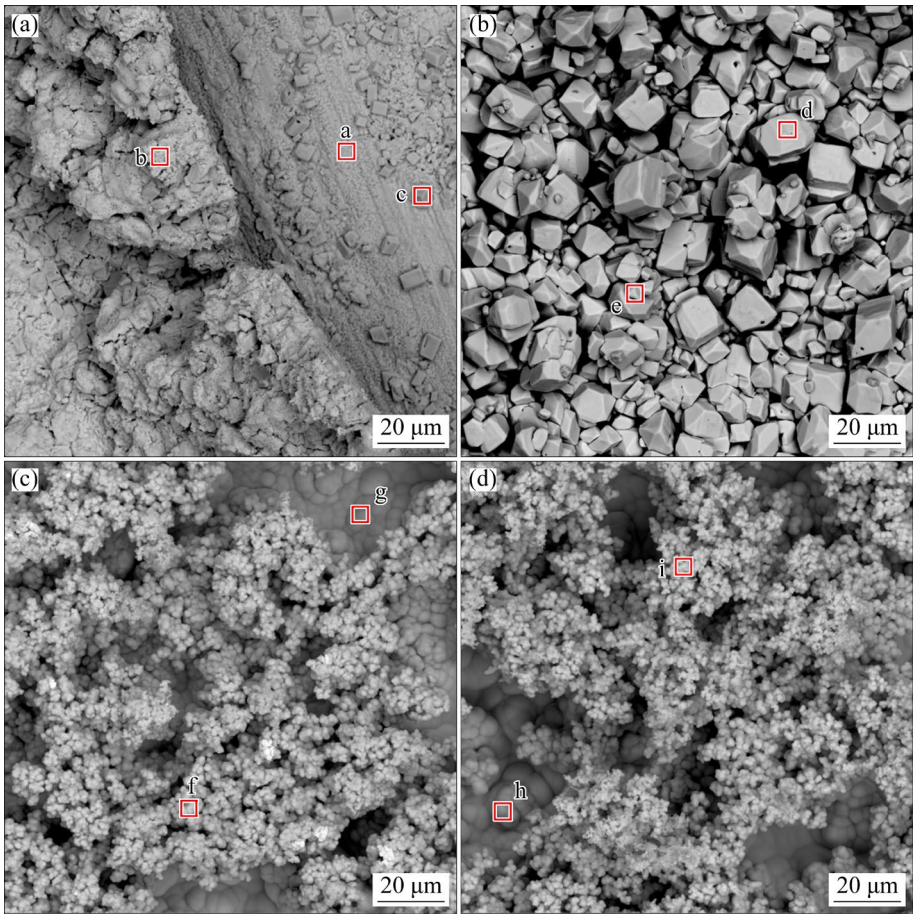

Fig. 8 SEM images of MRA (a, c) and DRA (b, d) before (a, b) and after (c, d) 24 h galvanostatic polarization at 500 A/m^2

anode [2]. If the anode is subjected to multiple mechanical injuries in the local area when the anode slime is manually removed for multiple times during the service period of zinc electrowinning, it may lead to the perforation of the anode local area and failure, which will seriously decrease the service life of the anode [32]. For DRA, the intact oxide layer not only effectively protects the anode from rapid corrosion, but also reduces the anodic oxygen evolution overpotential, which will significantly prolong the service life of the anode and reduce the power consumption of zinc electrowinning [8,26].

According to Section 3.1, the above analysis is consistent with the results of anodic mass loss and power consumption. As we all know, the zinc electrowinning electrolyte containing Mn^{2+} is conducive to protecting the anode from rapid corrosion [10,12]. Figures 8(c) and (d) show that the MnO_2 layer is formed on the MRA and DRA surface, while Fig. 8(b) exhibits that there exists an obvious lead-containing oxide layer on the anode surface, which indicates that the lead-containing oxide layer on MRA and DRA surface is completely covered by MnO_2 after 24 h of galvanostatic polarization. This is consistent with the reported experimental phenomenon [16]. Meanwhile, the loose coral like MnO_2 formed on the outer surface of the anode is prone to detachment and sedimentation to the bottom of the electrolytic cell due to poor adhesion, which is consistent with the phenomenon of anode slime at the bottom of the electrolytic cell in zinc electrowinning experiments.

3.3.2 Phase composition

To investigate the phase composition of each anode surface, XRD measurements were carried out and the results are illustrated in Fig. 10. MRA is mainly composed of $PbSO_4$ and PbO, while DRA is mainly composed of $PbSO_4$, α-PbO_2, β-PbO_2 and PbO. After 24 h of galvanostatic polarization at 500 A/m^2, MRA and DRA are both composed of α-MnO_2 and γ-MnO_2. The above XRD results are consistent with the SEM and EDS results of each

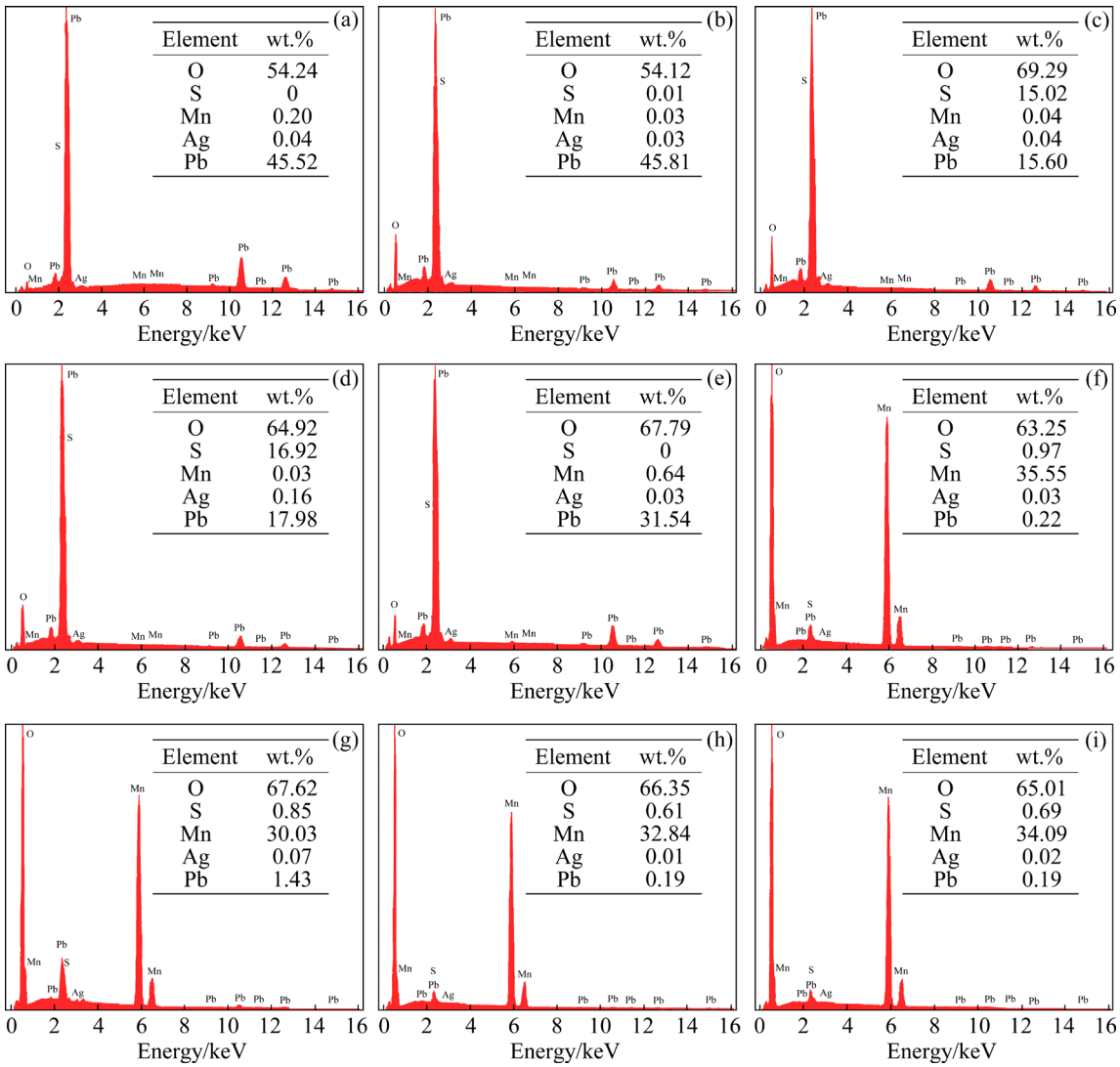

Fig. 9 EDS results corresponding to Fig. 8

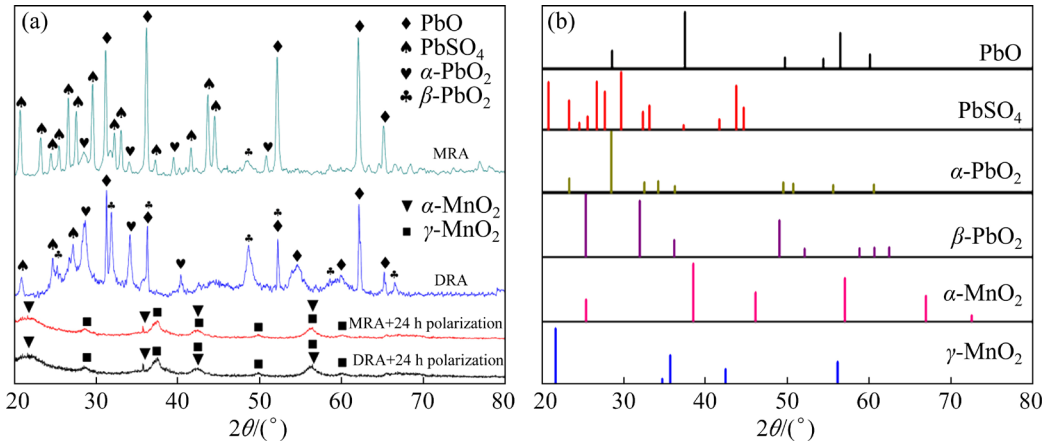

Fig. 10 XRD patterns of MRA and DRA before and after 24 h of galvanostatic polarization at 500 A/m^2: (a) Spectra of samples; (b) Standard spectra

anode. This indicates that different removing methods have a significant impact on the phase composition of the anode surface after slime removing, while they have almost no effect on the phase composition of the removed anode surface after 24 h of galvanostatic polarization.

For MRA, the Pb containing oxide film layer on the anode surface is extensively damaged in the manual removing process of anode slime due to mechanical damage on the anode surface, and only a portion of $PbSO_4$ is remained, thus the bare metal substrate on the anode surface is oxidized into PbO. Therefore, the surface of MRA is mainly composed of $PbSO_4$ and PbO. For DRA, only the manganese dioxide on the outer layer of anode surface is removed during the process of anode slime removing, while the lead oxide film in the inner layer of anode surface is completely retained [16,32]. Hence, the surface of DRA is mainly composed of $PbSO_4$, α-PbO_2, β-PbO_2 and PbO. For MRA and DRA after galvanostatic polarization, MnO_2 layer is formed on the anode surface, which blocks the lead oxide in the inner layer of the anode surface [16]. In that case, MRA and DRA are both composed of α-MnO_2 and γ-MnO_2 after galvanostatic polarization.

3.4 Application prospect

The traditional manual removing of anode slime in the zinc electrowinning process has disadvantages such as short anode service life, high power consumption in the early stage of service after slime removing, high cost of Pb pollution control, high manual labor intensity, and low removing efficiency. The Fe^{2+} dissolution method was applied to solving these problems, which have following excellent characteristics: (1) Fe^{2+} raw materials are easy to obtain and have low cost, thus leading to the low cost of anode slime removing; (2) it enables the effective protection of the anode surface oxide layer and metal substrate from mechanical damage, which is very helpful for extending the service life of anode and reducing the power consumption of zinc electrowinning after the anode slime is removed in the initial service period; (3) since the anodic surface oxide film is intact, it can effectively prevent Pb from contaminating the electrolyte, which not only helps enterprises reduce the cost on removing Pb from the electrolyte, but also obtains zinc products with lower Pb content; (4) the work load of workers, the number of workers and the labor cost of enterprises will be lower; (5) the simultaneous removing of anode slime on multiple anodes can be achieved, which can significantly improve the removing efficiency of anode slime in the zinc electrowinning process compared to traditional manual removing.

The removing of anode slime by Fe^{2+} dissolution method has obvious advantages over the traditional manual method in terms of power consumption, anode consumption cost, Pb pollution control, labor cost and removing efficiency. Nevertheless, the Fe^{2+} dissolution method will produce the solution containing Fe^{3+} and Mn^{2+} that are detrimental to the zinc electrowinning. The solution for this problem in industry is to purify the solution by zinc smelting for Fe removal and resource recovery.

4 Conclusions

(1) The anode corrosion rate of DRA is 57.14% lower than that of MRA due to the Pb-containing film layer, effectively inhibiting Pb pollution in the electrolyte, thus making the quality of zinc products in the initial service of the anode meet the $0^{\#}$ zinc standard. Meanwhile, the service life of the anode is significantly extended.

(2) The initial cell voltage and power consumption of DRA are 2.792 V and 2720 kW·h/t, respectively, which are considerably lower than those of MRA (3.346 V and 3142 kW·h/t) because the Pb-containing film layer has high oxygen evolution reaction catalytic activity.

CRediT authorship contribution statement

Wen-jun WANG: Conceptualization, Methodology, Investigation, Writing − Original draft; **Lan-bo LI:** Investigation, Formal analysis, Writing − Review & editing; **Xu LIU:** Conceptualization, Formal analysis, Visualization; **Tie-chui YUAN:** Validation, Writing − Review & editing, Supervision, Funding acquisition; **He-xin GAO:** Investigation, Formal analysis.

Declaration of competing interest

The authors declare that they have no known competing financial interests or personal relationships that could have appeared to influence the work reported in this paper.

Acknowledgments

This work was supported by Zhejiang Libo Industrial Co., Ltd., Shaoxing, China.

References

[1] SHAO Shuang, MA Bao-zhong, WANG Cheng-yan, CHEN Yong-qiang, ZHANG Wen-juan. A review on the removal of magnesium and fluoride in zinc hydrometallurgy [J]. Journal

of Sustainable Metallurgy, 2022, 8: 25−36.

[2] WANG Wen-jun, YUAN Tie-chui, LI Rui-di, WANG Zhuo-ran, LI Hai-hua, LI Lan-bo, ZHENG Dan. Electrochemical behaviors of powder-processed Pb−Ag anodes [J]. The Journal of the Minerals, Metals & Materials Society, 2019, 71: 2498−2504.

[3] LUO Jin, DUAN Ning, XU Fu-yuan, JIANG Lin-hua, ZHANG Chen-mu, YE Wan-qi. System-level analysis of the generation and distribution for Pb, Cu, and Ag in the process network of zinc hydrometallurgy: Implications for sustainability [J]. Journal of Cleaner Production, 2019, 234: 755−766.

[4] CHAI Li-yuan, YAN Xu, LI Qing-zhu, YANG Ben-tao, WANG Qing-wei. A comparative study of abiological granular sludge (ABGS) formation in different processes for zinc removal from wastewater [J]. Environmental Science and Pollution Research, 2014, 21: 12436−12444.

[5] YANG Chang-jiang. Polyoxometalate/lead composite anode for efficient oxygen evolution in zinc electrowinning [J]. Journal of the Electrochemical Society, 2019, 166(4): E129−E136.

[6] WANG Wen-jun, LI Rui-di, YUAN Tie-chui, ZHU Xian-yun, LI Hai-hua, LIN Wen-jun, LI Lan-bo. Effects of Ag^+ in diaphragm electrolysis on oxygen evolution and corrosion behaviors of Pb and Pb−Ag anodes [J]. Hydrometallurgy, 2020, 192: 105254.

[7] ZHONG Xiao-cong, ZHANG Bin, LIN Zhen-cong, LIU Jia-ming, XIE Yong-min, XU Zhi-feng. Preparation and performance of 3D-Pb anodes for nonferrous metals electrowinning in H_2SO_4 aqueous solution [J]. Transactions of Nonferrous Metals Society of China, 2020, 30: 535−547.

[8] WANG Wen-jun, YUAN Tie-chui, LI Rui-di, ZHU Xian-yun, LI Hai-hua, LIN Wen-jun, LI Lan-bo, ZHENG Dan. Electrochemical corrosion behaviors of Pb−Ag anodes by electric current pulse assisted casting [J]. Journal of Electroanalytical Chemistry, 2019, 847: 113250.

[9] YE Wan-qi, XU Fu-yuan, JIANG Lin-hua, DUAN Ning, LI Jian-hui, ZHANG Fei-long, ZHANG Ge, CHEN Lu-jun. A novel functional lead-based anode for efficient lead dissolution inhibition and slime generation reduction in zinc electrowinning [J]. Journal of Cleaner Production, 2021, 284: 124767.

[10] WANG Shuai, ZHOU Xiang-yang, MA Chi-yuan, LONG Bo, WANG Hui, TANG Jing-jing, YANG Juan. Electrochemical properties of Pb−0.6 wt.%Ag powder-pressed alloy in sulfuric acid electrolyte containing Cl^-/Mn^{2+} ions [J]. Hydrometallurgy, 2018, 177: 218−226.

[11] ZHONG Xiao-cong, YU Xiao-ying, JIANG Liang-xing, LV Xiao-juan, LIU Fang-yang, LAI Yan-qing, LI Jie. Influence of fluoride ion on the performance of Pb−Ag anode during long-term galvanostatic electrolysis [J]. The Journal of the Minerals, Metals & Materials Society, 2015, 67: 2022−2027.

[12] ZHANG Chen-mu, DUAN Ning, JIANG Lin-hua, XU Fu-yuan, LUO Jin. Influence of Mn^{2+} ions on the corrosion mechanism of lead-based anodes and the generation of heavy metal anode slime in zinc sulfate electrolyte [J]. Environmental Science and Pollution Research, 2018, 25: 11958−11969.

[13] CACHET C, LE PAPE-RÉROLLE C, WIART R. Influence of Co^{2+} and Mn^{2+} ions on the kinetics of lead anodes for zinc electrowinning [J]. Journal of Applied Electrochemistry, 1999, 29: 811−818.

[14] KARBASI M, KESHAVARZ ALAMDARI E. Investigation of lead base composite anodes produced by accumulative roll bonding [J]. Materials & Design, 2015, 67: 118−129.

[15] NIJJER S, THONSTAD J, HAARBERG G M. Oxidation of manganese (II) and reduction of manganese dioxide in sulphuric acid [J]. Electrochimica Acta, 2000, 46(2/3): 395−399.

[16] ZHANG Chen-mu, SHI Yao, JIANG Lin-hua, HU Ying-yan, LI Qiang, LI Hui-quan. Analysis of lead pollution control in anode slime micromorphology evolution induced by Mn^{2+} ions for cleaner production of zinc electrolysis [J]. Journal of Cleaner Production, 2021, 297: 126700.

[17] FAN Jin-long, WANG Gang, LI Qing, YANG Hao-wei, XU Shuo, ZHANG Jie, CHEN Jin-wei, WANG Rui-lin. Extraction of tellurium and high purity bismuth from processing residue of zinc anode slime by sulfation roasting−leaching−electrodeposition process [J]. Hydrometallurgy, 2020, 194: 105348.

[18] YE Wan-qi, XU Fu-yuan, JIANG Lin-hua, DUAN Ning, LI Jian-hui, MA Zi-zhen, ZHANG Fei-long, CHEN Lu-jun. Lead release kinetics and film transformation of Pb−MnO_2 pre-coated anode in long-term zinc electrowinning [J]. Journal of Hazardous Materials, 2021, 408: 124931.

[19] XU Rui-chao, JIANG Lin-hua, DUAN Ning, XU Fu-yuan, ZHANG Fei-long, ZHOU Chao, LI Wei-dong, LI Zhi-qiang. Research on microstructure of membrane-slime layer on lead-based anode surface in zinc hydrometallurgy by combining μ-XRF with mm-XRF [J]. Journal of Cleaner Production, 2022, 379: 134568.

[20] WANG Zhong-he, JIANG Yao, FENG Lu-li, HE Zhen-li, KANG Xi-yue, YU Ling-ping, HE Yue-hui, QIN Zi-jun, ZHAO Qian, QIU Yue, GAO Hai-yan. Synthesis and study of $TiMn_2$ intermetallic compound anode materials with different structures for zinc electrowinning [J]. Intermetallics, 2023, 161: 107989.

[21] SHEN Bo-tao, HE Yue-hui, LI Wen-hao, WANG Zhong-he, YU Lin-ping, JIANG Yao, LIU Xin-li, KANG Jian-gang, GAO Hai-yan, LIN Nan. Insight into electrochemical performance of porous Fe_xSi_y intermetallic anode for zinc electrowinning [J]. Materials & Design, 2020, 191: 108645.

[22] HE Shi-wei, XU Rui-dong, SUN Li, FAN You-qi, ZHAO Zhou, LIU Huan, LV Hui-hong. Electrochemical characteristics of Co_3O_4-doped β-PbO_2 composite anodes used in long-period zinc electrowinning [J]. Hydrometallurgy, 2020, 194: 105357.

[23] WANG Xuan-bing, WANG Jun-li, TONG Xiao-ning, WU Song, WEI Jin-long, CHEN Bu-ming, XU Rui-dong, YANG Lin-jing. Constructing of Pb−Sn/α-PbO_2/β-PbO_2−Co_2MnO_4 composite electrode for enhanced oxygen evolution and zinc electrowinning [J]. Materials Today Physics, 2023, 35: 101068.

[24] WANG Wen-jun, WANG Zhuo-ran, YUAN Tie-chui, LI Rui-di, LI Hai-hua, LIN Wen-jun, ZHENG Dan. Oxygen evolution and corrosion behavior of Pb−CeO_2 anodes in sulfuric acid solution [J]. Hydrometallurgy, 2019, 183:

221−229.
[25] MA Rui-xin, CHENG Shi-yao, ZHANG Xiao-yong, LI Shi-na, LIU Zi-lin, LI Xiang. Oxygen evolution and corrosion behavior of low-MnO_2-content Pb−MnO_2 composite anodes for metal electrowinning [J]. Hydrometallurgy, 2016, 159: 6−11.
[26] LI Hai-hua, YUAN Tie-chui, LI Rui-di. Electrochemical properties of powder-pressed Pb−Ag−PbO_2 anodes [J]. Transactions of Nonferrous Metals Society of China, 2019, 29: 2422−2429.
[27] LAI Yan-qing, JIANG Liang-Xing, LI Jie, ZHONG Shui-ping, LU Xiao-jun, PENG Hong-jian, LIU Ye-xiang. A novel porous Pb-Ag anode for energy-saving in zinc electrowinning: Part I. Laboratory preparation and properties [J]. Hydrometallurgy, 2010, 102: 73−80.
[28] LAI Yan-qing, JIANG Liang-xing, ZHONG Shui-ping, LU Xiao-jun, PENG Hong-jian, LIU Ye-xiang. A novel porous Pb−Ag anode for energy-saving in zinc electrowinning: Part II. Preparation and pilot plant tests of large size anode [J]. Hydrometallurgy, 2010, 102: 81−86.
[29] HUANG Hui, ZHOU Ji-yu, CHEN Bu-ming, GUO Zhong-cheng. Polyaniline anode for zinc electrowinning from sulfate electrolytes [J]. Transactions of Nonferrous Metals Society of China, 2010, 20(Suppl.): 288−292.
[30] WANG Wen-jun, YUAN Tie-chui, ZOU Li-hua, LI Hai-hua, LI Lan-bo, LI Rui-di. Effects of Co^{2+} in diaphragm electrolysis on the electrochemical and corrosion behaviors of Pb−Ag and Pb anodes for zinc electrowinning [J]. Hydrometallurgy, 2020, 195: 105412.
[31] ZHAO Duo-qiang, YANG Sheng-hai, CHEN Yong-ming, JIE Ya-fei, HE Jing, TANG Chao-bo. Effects of gelatin and polyoxyethylene ether on zinc electrowinning in a Zn(II)−NH_4Cl−H_2O system [J]. Hydrometallurgy, 2021, 201: 105567.
[32] ZHANG Fei-long, XU Fu-yuan, JIANG Lin-hua, ZUO Jia-ne, JIN Wei, YE Wan-qi, ZHUANG Si-wei, DUAN Ning. Dynamic evolution of structure–activity of anode on lead release and overpotential change in zinc electrowinning [J]. Chemical Engineering Journal, 2023, 451(3): 138944.
[33] STEFANOV Y S, VALCHANOVA I D, MAGAEVA S D, DOBREV T M. Investigations of composite coatings used as anodes for zinc electroextraction from sulphate electrolytes [J]. Bulgarian Chemical Communications, 2008, 40(3): 277−280.

Fe^{2+}溶蚀法清理阳极泥对 Pb−0.6%Ag 阳极电化学性能及锌电积的影响

王文军[1,2,3]，李澜波[1]，刘 旭[4]，袁铁锤[1]，高和欣[1]

1. 中南大学 粉末冶金国家重点实验室，长沙 410083；
2. 浙江力博实业股份有限公司，绍兴 312000；
3. 邵阳学院 机械与能源工程学院，邵阳 422000；
4. 株洲冶炼集团股份有限公司，株洲 412000

摘 要：对比研究 Fe^{2+}溶蚀法和人工法清理阳极泥对铸造 Pb−0.6%Ag(质量分数)阳极性能和锌电积的影响。结果表明，Fe^{2+}溶蚀法能避免阳极表面氧化膜层受到机械损伤，而传统人工法无法实现，这将使阳极腐蚀速率降低57.14%，从而减少电解液和锌产品的 Pb 污染。同时，相较于人工法，Fe^{2+}溶蚀法清理阳极泥可显著提高阳极的电催化活性，使阳极泥清理后的锌电积初始电耗低至 2720 kW·h/t。

关键词：Pb−Ag 阳极；锌电积；阳极泥清理；电化学性能

(Edited by Wei-ping CHEN)